HHS Public Access

Author manuscript

Neuroimage. Author manuscript; available in PMC 2016 August 15.

Published in final edited form as:

Neuroimage. 2015 August 15; 117: 114–123. doi:10.1016/j.neuroimage.2015.05.036.

Mapping the Functional Network of Medial Prefrontal Cortex by Combining Optogenetics and fMRI in Awake Rats

Zhifeng Liang[1,3,¶], **Glenn D.R. Watson**[2,3,¶], **Kevin D. Alloway**[2,3], **Gangchea Lee**[1], **Thomas Neuberger**[1,3], and **Nanyin Zhang**[1,3,*]

[1]Department of Biomedical Engineering, The Pennsylvania State University, University Park, PA 16802

[2]Neural and Behavioral Sciences, College of Medicine, The Pennsylvania State University, Hershey PA 17033

[3]Center for Neural Engineering, The Huck Institutes of Life Sciences, The Pennsylvania State University, University Park, PA, 16802

Abstract

The medial prefrontal cortex (mPFC) plays a critical role in multiple cognitive and limbic functions. Given its vital importance, investigating the function of individual mPFC circuits in animal models has provided critical insight into the neural basis underlying different behaviors and psychiatric conditions. However, our knowledge regarding the mPFC whole-brain network stays largely at the anatomical level, while the functional network of mPFC, which can be dynamic in different conditions or following manipulations, remains elusive especially in awake rodents. Here we combined optogenetic stimulation and functional magnetic resonance imaging (opto-fMRI) to reveal the network of brain regions functionally activated by mPFC outputs in awake rodents. Our data showed significant increases in blood-oxygenation-level dependent (BOLD) signals in prefrontal, striatal and limbic regions when mPFC was optically stimulated. This activation pattern was robust, reproducible, and did not depend on the stimulation period in awake rats. BOLD signals, however, were substantially reduced when animals were anesthetized. In addition, regional brain activation showing increased BOLD signals during mPFC stimulation was corroborated by electrophysiological recordings. These results expand the applicability of the opto-fMRI approach from sensorimotor processing to cognition-related networks in awake rodents. Importantly, it may help elucidate the circuit mechanisms underlying numerous mPFC-related functions and behaviors that need to be assessed in the awake state.

[*]Correspondence Author: Nanyin Zhang, Ph.D, Associate Professor, Department of Biomedical Engineering, The Huck Institutes of the Life Sciences, The Pennsylvania State University, W341 Millennium Science Complex, University Park, PA 16802, Tel: 814-8674791, nuz2@psu.edu.

[¶]Z.L. and G.W. equally contributed to this work.

Financial Disclosures:

Authors have no financial conflicts of interest.

Keywords

Opto-fMRI; medial prefrontal cortex; rat; awake

Introduction

In both humans and animals, the medial prefrontal cortex (mPFC) is a critical node in a distributed neural network (Ongur and Price, 2000) that regulates many cognitive and limbic functions such as working memory (Petrides, 1995), executive control (Ridderinkhof et al., 2004), decision making (Euston et al., 2012), and emotional learning (Milad and Quirk, 2012). Underscoring these functions, psychiatric disorders like schizophrenia (Chai et al., 2011; Eisenberg and Berman, 2010; Goghari et al., 2010) drug abuse (Goldstein and Volkow, 2011; Perry et al., 2011; Porrino and Lyons, 2000), post-traumatic stress disorder (Koenigs and Grafman, 2009; Shin et al., 2006) and major depression (Koenigs and Grafman, 2009; Myers-Schulz and Koenigs, 2012) have been attributed to mPFC dysfunction. Given its functional and clinical importance, investigating the function of individual mPFC circuits in animal models has provided insight into the neural basis of different behaviors and psychiatric conditions (Liang et al., 2014). For instance, selective activation or suppression of individual mPFC circuits in rodents has established the causal relationship between mPFC connectivity and depression-like behaviors (Warden et al., 2012). However, the mPFC whole-brain network is only studied at the anatomical level using tracing methods (Vertes, 2004), while the functional network of mPFC, which can be dynamic in different conditions and/or following manipulations, remains elusive, mainly due to the technical challenge of activating of mPFC while monitoring neural activity across the whole brain in animals. Lack of such knowledge highlights a critical gap to investigating interactions between individual mPFC circuits and their dynamics under different circumstances.

Functional magnetic resonance imaging (fMRI) has been widely used to map the sensory and motor functional networks in animals because of its superior spatial resolution and global view of brain activity (Zhang et al., 2008; Zhang et al., 2010b). However, fMRI is rarely used to reveal cognition-related networks in animals (Berns et al., 2012) for several reasons. In addition to the difficulty of administering cognitive tasks to animals during imaging, most animal fMRI studies have relied on anesthesia to immobilize animals, but cognitive processing is largely absent in the anesthetized state. Furthermore, anesthesia can alter both neural and vascular activities, and thus will significantly interfere with the fMRI signal (Martin et al., 2006).

To address these issues, we developed an alternative approach in which direct optogenetic stimulation of the mPFC is combined with fMRI (opto-fMRI) on awake animals. Compared to other stimulation approaches, optogenetics enables activation of specific populations of neurons at precise times (Yizhar et al., 2011). Hence, when combined with fMRI, optogenetic stimulation can determine how activity in a specific circuit element influences signaling throughout the rest of its interconnected network, and thus can derive causal relationships between different regions in a neural network (Lee et al., 2010).

Therefore, the current study used opto-fMRI to reveal the functional network that is activated by mPFC in rodents. To avoid the confounding effects of anesthesia, opto-fMRI was conducted in awake rats (Liang et al., 2011). A similar approach has been recently demonstrated in awake mice (Desai et al., 2011). An adeno-associated virus (AAV) that expresses channelrhodopsin (ChR2) was injected into mPFC, and after ChR2 expression occurred, mPFC was photo-activated during fMRI scanning. The global distribution of postsynaptic brain regions activated by mPFC was revealed by the pattern of significant fMRI signal increases throughout the brain. The reliability and dynamics of this network at different physiologic conditions were also examined.

Materials and Methods

Animals

Adult male Long-Evans (LE) rats (300–500g, Charles River Laboratories) were obtained from Charles River Laboratories. Animals were housed in Plexiglas cages (two per cage) and maintained on a 12 h light:12 h dark schedule in a room temperature of 22–24°C. Food and water were provided *ad libitum*. All procedures were approved by the Institutional Animal Care and Use Committee of the Pennsylvania State University.

Surgery

Each rat was anesthetized by intramuscular (IM) injections of ketamine (40 mg/kg) and xylazine (12 mg/kg). Atropine methyl nitrate (0.05 mg/kg) was injected IM to reduce bronchial secretions, and dexamethasone (0.5 mg/kg) was injected IM to prevent tissue inflammation. All rats were intubated through the oral cavity, placed in a stereotaxic frame (David Kopf Instruments, Tujunga, CA), and artificially ventilated with oxygen. Body temperature was maintained at 37°C with a heated water pad and a homeothermic heating blanket on the ventral and dorsal sides of the rat, respectively. After exposing the cranium surface, four plastic MR compatible screws (.080 × .125, nylon; PlasticsOne, Roanoke, VA) were placed along the temporal ridge. A small craniotomy was made unilaterally over the infralimbic (IL) subdivision of mPFC approximately 3 mm rostral and 0.5 mm lateral to bregma. A micropipette syringe fitted with a glass pipette tip (Hamilton Company, Reno, NV) was lowered through the craniotomy to inject 800–1200nl of AAV5.CaMKIIa.hChR2(H134R)-eYFP.WPRE.hGH (Addgene26969P, Penn Vector Core) into IL (4.4 – 4.7 mm ventral) at a rate of 60 nL/min. After the syringe was withdrawn, an optic fiber (0.4 mm diameter) embedded in a 2.5 mm ceramic ferrule (Thorlabs, 0.39 NA, Newton, NJ) was slowly advanced towards the injection site until it reached a depth of ~4.3 mm. Dental cement was applied around the screws and ceramic ferrule to create a chronic optic-fiber implant. Each rat was placed in its home cage for 3–4 weeks to allow the expression of ChR2 before starting acclimation to the MRI environment.

Optical stimulation setup

A laser (100 mW, 473 nm, Opto Engine LLC, Midvale, UT) was connected to a 7 meter long patch cable (Thorlabs, Ø400 μm core, 0.39 NA, Newton, NJ), which was attached to the optic-fiber stub implanted in the rat. The timing of the laser output was controlled by a National Instruments DAQ board (NI USB 6211, Austin, TX) with custom-written code in

LabView. Light power at the end of patch cable was set at 30mW as measured by a power meter (Thorlabs, Newton, NJ). Considering power loss due to the coupling between the patch cable and the implanted fiber stub, light power at the tip of the implanted fiber was estimated approximately 15 mW.

MR experiments

The timeline of the experimental procedures used in this study is summarized in Figure 1. As this figure indicates, all animals were acclimated to immobilization and the noise of the MRI scanning environment before imaging sessions were conducted using a paradigm documented in our earlier reports (Liang et al., 2011, 2012a, b, 2014; Liang et al., 2013; Liang et al., 2015; Zhang et al., 2010a). Each animal was gradually acclimated over a 7-day period to minimize motion and the stress that accompanies imaging in the awake state (King et al., 2005; Liang et al., 2014).

Each rat was imaged twice in the awake state and then once during anesthesia, and all of these imaging sessions were separated by at least two days. For anesthetized sessions, isoflurane (1–1.5%) was delivered to the animal through a nose cone, and the respiratory rate was monitored throughout the MRI experiment.

All imaging experiments were conducted on a 7T Agilent system (Agilent, Santa Clara, CA). During each MRI session, anatomical images were first acquired using a fast spin-echo multislice (fsems) sequence with the following parameters: repetition time (TR) = 2s; echo time (TE) = 40 ms; matrix size = 256×256; FOV = 3.2×3.2 cm; slice number = 20; slice thickness = 1 mm; and repetition number = 6. Gradient-echo images covering the whole brain were acquired using echo-planar imaging (EPI) with the following parameters: TR = 1 s; TE = 13.8 ms; matrix size = 64×64; FOV = 3.2×3.2 cm; slice number = 20; and slice thickness = 1 mm.

We used three different paradigms—two block designs and one event-related design—for the opto-fMRI experiments. In block design 1, the laser light was alternately turned on (10Hz, 10ms pulses) for 15 s and off for 30 s with a total of three light-on periods interleaved with four light-off periods. In block design 2, the laser light was alternately turned on for 30s (10Hz, 10ms pulses) and off for 30s with three light-on periods interleaved with four light-off periods. For the event-related design, each epoch consisted of a light flash for 1s (20Hz, 10ms pulses) and an inter-stimulus interval of 30s. A total of 10 epochs were delivered for each scan. In each paradigm, light pulse delivery was triggered by a TTL signal from the MR console at the beginning of each opto-fMRI scan.

Data analysis

Anatomical images were first manually aligned to a fully segmented rat brain atlas in Medical Image Visualization and Analysis (MIVA, ccni.wpi.edu). EPI images were motion-corrected using the realign function in SPM8 (http://www.fil.ion.ucl.ac.uk/spm/), and spatially smoothed (FWHM 1mm). Motion parameters were regressed out from the time course of each voxel, and then voxel time courses were linearly detrended. The first ten volumes of EPI images were discarded to allow the magnetization to reach steady state.

The subsequent series of procedures for analyzing preprocessed opto-fMRI data are summarized in Figure 2. Because the hemodynamic response function (HRF) of the optogenetically generated blood-oxygenation-level dependent (BOLD) signal is not well characterized, we adopted a Fourier analysis paradigm that does not assume a particular HRF (Lee et al., 2010). For each individual voxel, the time series was Fourier transformed to the frequency domain, and the coherence value (c value) was calculated as defined in the following equation:

$$c=\frac{|F(f_0)|}{\sqrt{\sum_f |F(f)|^2}}$$

where $|F(f_0)|$ is magnitude of the stimulation frequency component, and $\sqrt{\sum_f |F(f)|^2}$ is the sum of squares of magnitudes of all frequency components. Coherence values were further converted to z values using the following equation:

$$z=\frac{1}{\sigma}\left(\sqrt{\frac{c^2}{(1-c^2)}\left((N-1)\sigma^2+Nm^2\right)}-m\right)$$

where m is the mean, σ^2 is the variance, and N is the sample size for estimation of m and σ. z value images were calculated for all scans, and were subsequently averaged across individual conditions (i.e. awake or anesthetized) to yield the mean z image for each condition.

To threshold the z images, we adopted an adaptive thresholding strategy developed by Allen et al. (Allen et al., 2011). The distribution of z values represents a mixture of Normal and Gamma distributions. It is assumed that z values associated with optogenetic activation follow the Gamma distribution, while the remaining z values follow the Normal distribution. Thus, all z values from each mean z image were fitted by a Normal-Gamma mixture model defined as follows:

$$p(z)=c*N(z|\mu,\sigma)+(1-c)*G(z-\mu|\alpha,\beta)$$

where *N(.)* indicates Normal distribution and *G(.)* indicates Gamma distribution. c, μ, and σ^2 are the proportion, mean, and variance of Normal distribution, respectively. α and β are two parameters of Gamma distribution. Five parameters (c, μ, σ, α and β) were estimated by minimizing the residual sum of square errors between the fitted and empirical distributions using the *lsqnonlin* function in Matlab (Mathworks, Inc., Sherborn, MA). The fitting was separately performed on the mean z image of each condition, and the z value threshold was set based on the estimated mean and variance of Normal distribution for the condition (e.g. a threshold of $z > \mu + 3\sigma$ corresponds to a p value of 0.001 for mean z images).

To statistically compare the BOLD activation maps between the awake and anesthetized conditions, a linear mixed effect model (implemented in *fitlme* function in Matlab) was

applied to z-value maps of all sessions with conditions (awake or anesthetized) as the fixed effect and animals as the random effect. For each individual voxel, a t value and p value were generated, and $p<0.001$ (uncorrected) was deemed statistically significant.

Electrophysiology

Some rats were used in electrophysiology experiments after MR imaging was complete. The main purpose was to determine if photo-activation of IL cortex evoked increases in neuronal discharges in the postsynaptic target regions that displayed increases in BOLD signals during opto-fMRI. A secondary purpose was to determine if direct photostimulation of those target sites could evoke extracellular discharges, presumably by activating ChR2-expressing terminal projections from IL cortex.

Rats used for electrophysiology were anesthetized and stabilized as previously described in the surgical section. A flat machine screw was placed over the cerebellum to provide a ground lead for neuronal recordings. The dental acrylic was carefully removed to allow additional craniotomies for inserting optrodes or conventional electrodes at the lateral habenula (LHb; −3.0 mm rostral, 0.7 mm lateral to bregma) or the anterior cingulate cortex (AC; −1.0 mm rostral, 0.6 mm lateral to bregma). In some cases the chronically-implanted optic fiber was carefully removed and was replaced with an optrode so that ChR2-expressing neurons in IL cortex could be recorded during photostimulation.

In all electrophysiology experiments, a patch cable connected to the laser light source (473 nm) was attached either to the chronically implanted optic fiber or to an optrode inserted in its place. Extracellular discharges were amplified (Dagan 2200; Dagan Corp., Minneapolis, MN) and monitored on a digital oscilloscope (Tektronix DPO4034; Tektronix Beaverton, OR) connected to an acoustic speaker. The analog voltage signals were converted into digital signals (DT2839, Data Translation, Marlboro, MA) that were sampled at a rate of 26 kHz using a DataWave SciWorks data acquisition system (DataWave Technologies, Loveland, CO).

Histology

After the electrophysiological experiment, rats were deeply anesthetized with an IM injection of ketamine (60 mg/kg) and xylazine (18 mg/kg), and were then transcardially perfused with physiological saline followed by 4% paraformaldehyde in 0.1 M phosphate buffer saline and 4% paraformaldehyde containing 10% sucrose. Excised brains were stored in 4% paraformaldehyde with 30% sucrose for 3 days, and then the brain was cut coronally on a freezing microtome into 60-μm sections. Alternate, serially-ordered sections were mounted on gel-coated slides and dried overnight before being processed for thionin or used for fluorescent microscopy. Glass cover slips were placed over mounted sections with Cytoseal.

The coronal sections were used to visualize ChR2 expression at the IL injection site and at projection targets throughout the brain. We examined the brain for “tracks” produced by chronically-implanted optic fibers, recording electrodes, or stimulating/recording optrodes to insure that these were in regions that displayed CHR2 expression. Fluorescent microscopy was used to confirm ChR2 expression using a 51004v2 FITC/TRITC filter cube (Chroma

Technology Corp, Bellows Falls, VT) for widefield fluorescence microscopy on an Olympus BH2 microscope fitted with several objectives.

Results

A total of 11 rats were used in this study, in which 10 rats received AAV injections and were chronically implanted with an optic fiber in IL cortex. Among these 10 rats, only 7 underwent imaging sessions. The other 3 rats were not used because the optic-fiber stub either became loose or was dislodged before imaging. Four of the rats that completed all three imaging sessions were subsequently used for electrophysiology recording experiments. One additional rat was used to evaluate the potential heating effect of laser light in the brain. This rat was chronically implanted with an optic fiber in IL cortex but did not receive AAV injection.

Opto-fMRI activation patterns

Optical stimulation of mPFC revealed an extensive network of activated brain regions in the awake rat. In contrast, the spatial extent of this functional network was rather limited in the anesthetized rat. As indicated by Figure 3, BOLD activation maps ($p<0.05$ at whole-brain level) averaged across all three (two block and one event-related) paradigms in all animals displayed substantial differences in the mPFC-activated networks obtained from awake (Fig. 3a) and anesthetized (Fig. 3b) rats. Prominent increases in BOLD signals were observed around the tip of the optic fiber in both the awake and anesthetized states, but postsynaptic targets of IL cortex activated by IL photo-stimulation were largely limited in the insula and orbital cortex (OC) when animals were anesthetized. By contrast, IL photo-stimulation in the awake state evoked BOLD signal increases in widely distributed regions including the anterior cingulate (AC), prelimbic (PrL), and orbital cortices. Additional BOLD signal increases were also observed in subcortical regions such as the caudate putamen (CPu), septum, nucleus accumbens (NAc), bed nucleus of the stria terminalis (BST), the habenula (Hb), the medial dorsal nucleus of the thalamus (MD), and the hypothalamus. Importantly, all of the regions exhibiting increased BOLD signals receive projections from the IL cortex (Vertes, 2004). Interestingly, most limbic and striatal regions showed ipsilateral activations, whereas the prefrontal regions and thalamus showed bilateral activations in response to unilateral IL photo-stimulation. These hemispheric patterns of postsynaptic activations are also consistent with previous tracer studies (Vertes, 2004).

Voxel-wise statistical comparisons of BOLD maps between the awake and anesthetized conditions further confirm significantly stronger activation in widely spread regions in the awake rat (Fig. 3c).

In addition to displaying more spatially-distributed activations than anesthetized rats, awake rats were characterized by higher BOLD signal amplitudes. Figure 4 shows regionally averaged time courses of AC for each paradigm in both awake and anesthetized rats. The ROI was anatomically defined using a segmented atlas (Liang et al., 2013) based on the Swanson atlas (Swanson, 2004). Time courses were extracted by averaging all voxels within the ROI. Regardless of the photo-stimulation paradigm that was used, robust BOLD signal increases that followed the corresponding stimulation period were consistently observed in

the awake state. The magnitude of the BOLD signal increases in AC were approximately 3–4% for block paradigms and 2% for the event-related paradigm. In the anesthetized state, by contrast, BOLD signal increases in AC were considerably weaker, and the peak BOLD magnitudes were less than 1% for all stimulation paradigms. Taken together, these data indicate that photo-stimulation of IL evoked significantly stronger activations in the awake state. This result is also consistent with the opto-fMRI study conducted in awake mice (Desai et al., 2011).

Reliability of opto-fMRI data

Subsequently, we evaluated the inter-subject variability of the opto-fMRI data. Figure 5a demonstrates BOLD activation maps averaged from the two awake sessions for each individual animal. Fig. 5b displays voxel-wise correlations of z values between these individual BOLD maps and the mean activation map from all animals (i.e. Fig. 3a). Importantly, the activation patterns were consistent across animals (Figure 5a), and individual BOLD maps were all highly correlated with the mean activation map (Fig. 5b, $p<10^{-20}$ for all rats). These data suggest that the mPFC functional network revealed by opto-fMRI was robust.

To further assess the reproducibility between the two awake imaging sessions acquired in the same animal, the opto-fMRI data between the two sessions were compared. As indicated by Figure 6, the BOLD activation map averaged from the first sessions in all rats exhibited consistent spatial patterns with that averaged from the second sessions in all rats. In addition, z values of the corresponding voxels in the two maps were highly correlated ($r = 0.79$, $p<10^{-20}$). Moreover, the voxel-wise correlations between the two sessions were also very high for all individual animals (Table 1 in Supplemental Information, $p<10^{-20}$ for all rats), further indicating a high degree of reproducibility of the activation patterns.

We also evaluated the consistency of the activation patterns obtained between the block and event-related paradigms. As demonstrated in Figure 1 in Supplemental Information, although the exact pattern of activation depended on the state of the animal, within each state the spatial BOLD activation patterns were consistent across both types of stimulation paradigms. The voxel-to-voxel correlation coefficient between activation maps obtained in the block and event-related paradigms was $r = 0.58$ ($p<10^{-20}$) in the awake state and $r= 0.61$ ($p<10^{-20}$) in the anesthetized state.

Collectively, these results indicate that the BOLD activation patterns evoked by IL photo stimulation were robust and highly reproducible. The activation patterns did not depend on the duration of the photo-stimulation periods. Nevertheless, the magnitude and spatial distribution of BOLD responses were significantly different between the awake and anesthetized states.

Neuronal responses to photo-stimulation of IL cortex

In four rats underwent opto-fMRI, neuronal responses to photo-stimulation were subsequently recorded at sites that displayed significant increases in BOLD signals. As illustrated for one of these cases in Figure 7, photo-stimulation during opto-fMRI evoked a significant increase in BOLD signals at the site where the optic fiber was implanted in IL

cortex (Fig. 7A). Several postsynaptic targets of IL cortex also showed increases in BOLD signals during IL optical stimulation, including the habenula and mediodorsal region in the thalamus (Hb-MD, Fig. 7D), and the AC (Fig 7G).

One week after completing opto-fMRI, the animal was used to record photo-evoked neuronal responses simultaneously from IL cortex and its postsynaptic target in the Hb-MD thalamic region. In these animals, the chronically-implanted optic fiber was removed and an optrode, consisting of an optic fiber glued onto a tungsten electrode, was inserted in its place. The optrode allowed us to photo-stimulate IL cortex while simultaneously recording extracellular discharges of the local ChR2-expressing neurons that respond to light (Fig. 7B). In addition, a second tungsten electrode was then advanced into the Hb-MD thalamic region while light pulses were delivered by the optrode in IL cortex.

Among the four animals tested, neuronal responses were successfully recorded from two of them. As shown in Figure 7, photo-activation of IL cortex evoked neuronal discharges in both IL cortex and at multiple recording depths within the Hb-MD region,. Although the IL neuron displayed a high rate of spontaneous activity (~30 discharges/sec), each 50-ms light pulse evoked a brief, yet noticeable increase in activity that was followed by a longer period in which spontaneous activity was almost completely suppressed (Fig. 7B). The neuron recorded simultaneously in the Hb-MD region had a lower rate of spontaneous activity (~15 discharges/sec) and responded to IL photo-stimulation with a four-fold increase in discharge rate that returned to spontaneous levels as soon as each light pulse ended (Fig 7C).

In these two rats we recorded a total of five Hb-MD neurons during optical stimulation of ChR2-expressing neurons in IL cortex. In all five instances, the Hb-MD neurons displayed excitatory responses that averaged 48.9 spikes/sec (+/−3.5, SEM) above the spontaneous discharge rate. The mean latency of these responses to IL stimulation was 7.8 ms (+/− 0.73 ms). Histological examination of the electrolytic microlesion marking the recording sites in both of these cases indicated that the recorded neurons were in the Hb-MD region (see Fig. 7F).

In one rat, after recording light-evoked responses simultaneously in IL and Hb-MD, the optrode was removed from IL cortex and was inserted into AC, which receives axonal projections from IL cortex (Vertes, 2004). In this case, the optrode was aimed at the cingulate site that showed significant increases in BOLD signals when IL cortex was photo-stimulated during opto-fMRI (Fig. 7G). As the optrode was advanced into AC, light pulses were periodically delivered to evoke an increase in neuronal discharges. When photo-activated neuronal responses were encountered in AC, the optrode remained at this site while we administered a block of photo-stimulation trials. As indicated by the PSTH in Fig. 7H, repeated photo-stimulation at three recording sites in cingulate cortex of this animal revealed an increase in neuronal responsiveness that averaged 39.2 (+/− 6.8) spikes/sec above spontaneous activity. Presumably, these extracellular responses were mediated by photo-activation of ChR2-expressing terminals that released an excitatory neurotransmitter that, in turn, activated the postsynaptic neurons recorded by the optrode. Consistent with this multi-step process, the initial increase in the neuronal discharge rate had a mean latency of 4.0 (+/− 1.0) ms.

After passing electric current through the tungsten electrode to mark the recording site, histological examination revealed a microlesion ventral to a vertical shaft of damage produced by the dorsally-located optic-fiber. The tissue between the microlesion and the damage produced by the optic-fiber appeared normal, and this suggests that the tissue was not altered by heat or other “side effects” of the light pulses.

These results demonstrate that regional BOLD signal increases during opto-fMRI experiments was corroborated by electrophysiological recordings and, furthermore, these functional interactions corroborate anatomical reports on IL efferent projections (Vertes, 2004).

Discussion

The present study revealed the functional network of mPFC in the awake rat by optogenetically stimulating the IL subdivision of mPFC while simultaneously monitoring fMRI responses across the whole brain. We observed robust BOLD activations in prefrontal, striatal and limbic regions as IL was optically stimulated. This activation pattern was robust, reproducible, and did not depend on the specific parameters of the experimental paradigm. In addition, the presumption that regional increases in BOLD signals during IL stimulation are due to neuronal activation was corroborated by subsequent electrophysiological recordings. To our knowledge, this work is the first study to probe distributed functional networks of higher-order, cognition-related brain regions in awake rodents.

The present study is significant in two aspects. First, it demonstrates the feasibility of combining optogenetics and fMRI in awake rats. Previously there was only one opto-fMRI study that was conducted in awake mice (Desai et al., 2011). Second, it uncovered the cognition-related network activated by mPFC. This is different from the previous opto-fMRI study in awake mice that focused on the sensorimotor system (Desai et al., 2011). Comparing to the anatomical circuits revealed by tracing studies, mapping the mPFC neural network activated in awake animals offers the opportunity for understanding dynamic interactions between connected brain regions and how this neural network is reconfigured in different conditions or following manipulations that lead to neuroplasticity. As a result, opto-fMRI in awake rats is a valuable tool for investigating the circuit-level mechanisms that underlie numerous mPFC-related brain functions and behaviors.

The functional network of mPFC in awake rodents revealed by opto-fMRI

Optogenetics has opened a new avenue for interrogating the neural circuit mechanisms that mediate many behaviors (Deisseroth et al., 2006). The scientific value of this technique is tremendously expanded by combining it with fMRI, because photo-activating a specific circuit element reveals how it interacts with the rest of the interconnected network (Lee et al., 2010). Furthermore, opto-fMRI does not suffer from the issue of electromagnetic related artifacts encountered by conventional electrical stimulation approaches.

The feasibility of opto-fMRI in isoflurane-anesthetized rats was first demonstrated when projection neurons in primary motor cortex and thalamus were optogenetically activated while both local and distant BOLD signals were imaged throughout the brain (Lee et al.,

2010). Similar opto-fMRI studies examined the hippocampal connectivity of anesthetized rats (Abe et al., 2012), the somatosensory system of awake mice (Desai et al., 2011), as well as the visual system in anesthetized primates (Gerits et al., 2012). In addition, opto-fMRI was used to investigate neurovascular coupling (Kahn et al., 2013; Scott and Murphy, 2012), and it revealed the linearity of optically-evoked BOLD responses (Kahn et al., 2013). Overall, these studies demonstrate that optical stimulation of ChR2-expressing neurons can evoke robust neuronal responses detected by fMRI (Li et al., 2011b).

Despite the success of the opto-fMRI approach in mapping sensorimotor systems, its ability to reveal the full extent of a cognitive network in awake animals has never been demonstrated. This capacity is critically important because it can help reveal the site of neuroplasticity in functional networks that are altered by cognitive and behavioral conditioning or by stimuli that have a cognitive impact. To achieve this goal, a critical step is to use opto-fMRI to map the neural network that is activated during cognitive processing in the awake animal, not only because anesthesia alters neural and vascular activities (Liang et al., 2012a, b; Liang et al., 2015; Lu et al., 2007), but also because cognition requires an awake state. In the present study, opto-fMRI revealed the whole-brain functional network activated by mPFC, but only in the awake state. The spatial pattern of brain activation was generally consistent with the connectional projections of mPFC revealed by tracer studies (Vertes, 2004). Specifically, unilateral photo-stimulation of IL cortex induced bilateral activations in AC, PL, OC, RSC, MD and Hb, as well as ipsilateral activations in the striatum, septum, NAc, BST and hypothalamus.

Separate mPFC connections involved in various behaviors

The mPFC network revealed here consisted of several circuits that are reportedly involved in different functions and behaviors. Consistent with previous findings (Hoover and Vertes, 2007; Liang et al., 2013; Vertes, 2004), our results showed that many frontal areas are strongly interconnected. The strong connections within these frontal areas suggest that information received and processed by PFC has an influence on other prefrontal areas when mediating various cognitive and limbic functions (Euston et al., 2012). In addition, IL cortex provides input to the lateral Hb (Vertes, 2004), and this agrees with our results showing that IL photo-stimulation induced significant BOLD activation and electrophysiological responses in the Hb-MD region. This is significant because this connection is reportedly involved in learned responses to pain, stress, anxiety and reward (Hikosaka, 2010; Li et al., 2011a).

We detected the neural connection between ventral mPFC and the hypothalamus, which subserves intrinsic homeostatic drives and coordinates the autonomic and endocrine systems (Saper, 2003). We also observed strong connections between IL and the anterior insular areas, which are involved in interoception (Allen et al., 1991). Insula receives convergent visceral and limbic input (Allen et al., 1991; Ruggiero et al., 1987; Saper, 1982), and it may represent a major source of viscerosensory information to IL. Lastly, IL photo stimulation evoked unilateral activation in the ventral striatum, and this is consistent with data showing that the ventral mPFC sends unilateral projections to the ventromedial striatum (Gabbott et al., 2005), which is involved in emotional learning (Do-Monte et al., 2013).

These results indicate that opto-fMRI can simultaneously map multiple mPFC circuits in awake, but not anesthetized rodents. This is important for understanding the functional role of individual mPFC circuits in separate types of animal behaviors, as most behavioral-cognitive assessments are done in the awake state. Hence, opto-fMRI conducted on awake rats has the potential to provide important insights for revealing the functional circuit mechanisms that mediate neuroplasticity induced by mPFC-related behaviors.

Reliability of the mPFC network revealed by opto-fMRI

Our results showed that the BOLD activation patterns evoked by IL photo-stimulation were robust in both the awake and anesthetized states but were significantly altered between the two states. First, BOLD time courses followed the stimulation periods very tightly. Second, BOLD activation patterns were consistent across animals (Fig. 5). Third, BOLD activities in response to IL stimulation were highly reproducible, supported by a high voxel-to-voxel correlation between the BOLD activation maps from two awake opto-fMRI sessions at both the group level (Fig. 6) and individual level (Table 1 in Supplemental Information). Finally, BOLD activation patterns were consistent across all of our stimulation paradigms (Supplemental Figure 1). These results collectively suggest that IL photo stimulation induced robust responses across the mPFC network.

Notably, an adaptive thresholding method (Allen et al., 2011) was adopted in the current study. By choosing statistical thresholds based on model fitting of each statistical image, this method accounted for different variances in different conditions. For example, the thresholds in absolute z values were higher for longer stimulation periods (i.e. 15 and 30s) than shorter stimulation (i.e. 1s) at the same levels of statistical significance. This result indicates that larger variances were present during prolonged stimulations. Therefore, as applied in the present study, the adaptive thresholding strategy offers advantages over other thresholding methods that use single z values for multiple conditions.

Potential influences of motion and heating during optical stimulations on BOLD maps

Motion is a confounding factor that can potentially induce artifactual BOLD activations in fMRI experiments. To control for motion artifacts, functional images were realigned with the SPM realignment function, and all six motion parameters were regressed out from the BOLD time course of each individual voxel in our data preprocessing. To further evaluate the potential influence of residual movement on the BOLD maps evoked by optical stimulation of mPFC particularly in the awake rat, we analyzed the correlations between animals' movement and the BOLD time series of individual voxels. Supplemental Figure 2 shows the averaged map of the correlation coefficient between the volume-to-volume displacement and the BOLD time series of each individual voxel. The data indicate that this correlation was very weak across the whole brain, and no significant spatial patterns were observed. This result suggests that motion did not significantly contribute to the map of BOLD signals evoked by optically stimulating mPFC in awake rats.

It has been suggested that the heating effect generated by blue laser light can create artifactual BOLD activations around the optical fiber tip area, where the light is delivered (Christie et al., 2013; Desai et al., 2011). To evaluate this potential heating effect, one

control rats was chronically implanted with an optic fiber in IL cortex but did not receive AAV injection. This rat was imaged in two separate opto-fMRI sessions in the awake state using the same laser power. Supplemental Figure 3 shows the regionally averaged BOLD time series at the optical fiber tip area (15 voxels, top panel) and AC (bottom panel), respectively. No appreciable BOLD activation was observed in either region. This result suggests that the potential heating effect on our results was negligible, likely due to the combination of low duty cycle (10% for 15 and 30s stimulation and 20% for 1s stimulation) and a relatively large optical fiber diameter which generated low light power per unit area (~119 mw/mm^2).

Conclusions

This study combined optogenetics and fMRI to uncover the functional neural network that was activated when mPFC was optogenetically stimulated. The results revealed robust and reproducible activations in local and distant brain regions that receive inputs from mPFC. Furthermore, neural activation in several of the regions was confirmed by subsequent electrophysiology recordings. Using opto-fMRI in awake rats represents a new direction for investigating the global brain networks that subserve cognitive and limbic functions. If used in conjunction with behavioral testing in the future, this approach has even greater potential for determining how behavior is linked to global changes in neural activity throughout spatially-distributed neural systems, which may include regions that are inaccessible with conventional techniques.

Supplementary Material

Refer to Web version on PubMed Central for supplementary material.

Acknowledgments

Authors would like to thank Drs. Gregory Quirk and Bruce McEwen for their helpful scientific discussions, and Drs. Christopher Moore and Karel Svoboda for helping us implement optogenetics in our laboratories. This work was supported by the National Institutes of Health Grant Numbers R01MH098003 (PI: Nanyin Zhang, PhD) from the National Institute of Mental Health and R01NS085200 (PI: Nanyin Zhang, PhD) from the National Institute of Neurological Disorders and Stroke.

References

Abe Y, Sekino M, Terazono Y, Ohsaki H, Fukazawa Y, Sakai S, Yawo H, Hisatsune T. Opto-fMRI analysis for exploring the neuronal connectivity of the hippocampal formation in rats. Neurosci Res. 2012; 74:248–255. [PubMed: 22982343]

Allen EA, Erhardt EB, Damaraju E, Gruner W, Segall JM, Silva RF, Havlicek M, Rachakonda S, Fries J, Kalyanam R, Michael AM, Caprihan A, Turner JA, Eichele T, Adelsheim S, Bryan AD, Bustillo J, Clark VP, Feldstein Ewing SW, Filbey F, Ford CC, Hutchison K, Jung RE, Kiehl KA, Kodituwakku P, Komesu YM, Mayer AR, Pearlson GD, Phillips JP, Sadek JR, Stevens M, Teuscher U, Thoma RJ, Calhoun VD. A baseline for the multivariate comparison of resting-state networks. Front Syst Neurosci. 2011; 5:2. [PubMed: 21442040]

Allen GV, Saper CB, Hurley KM, Cechetto DF. Organization of visceral and limbic connections in the insular cortex of the rat. J Comp Neurol. 1991; 311:1–16. [PubMed: 1719041]

Berns GS, Brooks AM, Spivak M. Functional MRI in awake unrestrained dogs. PLoS One. 2012; 7:e38027. [PubMed: 22606363]

Chai XJ, Whitfield-Gabrieli S, Shinn AK, Gabrieli JD, Nieto Castanon A, McCarthy JM, Cohen BM, Ongur D. Abnormal medial prefrontal cortex resting-state connectivity in bipolar disorder and schizophrenia. Neuropsychopharmacology. 2011; 36:2009–2017. [PubMed: 21654735]

Christie IN, Wells JA, Southern P, Marina N, Kasparov S, Gourine AV, Lythgoe MF. fMRI response to blue light delivery in the naive brain: implications for combined optogenetic fMRI studies. Neuroimage. 2013; 66:634–641. [PubMed: 23128081]

Deisseroth K, Feng G, Majewska AK, Miesenbock G, Ting A, Schnitzer MJ. Next-generation optical technologies for illuminating genetically targeted brain circuits. J Neurosci. 2006; 26:10380–10386. [PubMed: 17035522]

Desai M, Kahn I, Knoblich U, Bernstein J, Atallah H, Yang A, Kopell N, Buckner RL, Graybiel AM, Moore CI, Boyden ES. Mapping brain networks in awake mice using combined optical neural control and fMRI. J Neurophysiol. 2011; 105:1393–1405. [PubMed: 21160013]

Do-Monte FH, Rodriguez-Romaguera J, Rosas-Vidal LE, Quirk GJ. Deep brain stimulation of the ventral striatum increases BDNF in the fear extinction circuit. Front Behav Neurosci. 2013; 7:102. [PubMed: 23964215]

Eisenberg DP, Berman KF. Executive function, neural circuitry, and genetic mechanisms in schizophrenia. Neuropsychopharmacology. 2010; 35:258–277. [PubMed: 19693005]

Euston DR, Gruber AJ, McNaughton BL. The role of medial prefrontal cortex in memory and decision making. Neuron. 2012; 76:1057–1070. [PubMed: 23259943]

Gabbott PL, Warner TA, Jays PR, Salway P, Busby SJ. Prefrontal cortex in the rat: projections to subcortical autonomic, motor, and limbic centers. J Comp Neurol. 2005; 492:145–177. [PubMed: 16196030]

Gerits A, Farivar R, Rosen BR, Wald LL, Boyden ES, Vanduffel W. Optogenetically induced behavioral and functional network changes in primates. Curr Biol. 2012; 22:1722–1726. [PubMed: 22840516]

Goghari VM, Sponheim SR, MacDonald AW 3rd. The functional neuroanatomy of symptom dimensions in schizophrenia: a qualitative and quantitative review of a persistent question. Neurosci Biobehav Rev. 2010; 34:468–486. [PubMed: 19772872]

Goldstein RZ, Volkow ND. Dysfunction of the prefrontal cortex in addiction: neuroimaging findings and clinical implications. Nat Rev Neurosci. 2011; 12:652–669. [PubMed: 22011681]

Hikosaka O. The habenula: from stress evasion to value-based decision-making. Nat Rev Neurosci. 2010; 11:503–513. [PubMed: 20559337]

Hoover WB, Vertes RP. Anatomical analysis of afferent projections to the medial prefrontal cortex in the rat. Brain Struct Funct. 2007; 212:149–179. [PubMed: 17717690]

Kahn I, Knoblich U, Desai M, Bernstein J, Graybiel AM, Boyden ES, Buckner RL, Moore CI. Optogenetic drive of neocortical pyramidal neurons generates fMRI signals that are correlated with spiking activity. Brain Res. 2013; 1511:33–45. [PubMed: 23523914]

King JA, Garelick TS, Brevard ME, Chen W, Messenger TL, Duong TQ, Ferris CF. Procedure for minimizing stress for fMRI studies in conscious rats. J Neurosci Methods. 2005; 148:154–160. [PubMed: 15964078]

Koenigs M, Grafman J. The functional neuroanatomy of depression: distinct roles for ventromedial and dorsolateral prefrontal cortex. Behav Brain Res. 2009; 201:239–243. [PubMed: 19428640]

Lee JH, Durand R, Gradinaru V, Zhang F, Goshen I, Kim DS, Fenno LE, Ramakrishnan C, Deisseroth K. Global and local fMRI signals driven by neurons defined optogenetically by type and wiring. Nature. 2010; 465:788–792. [PubMed: 20473285]

Li B, Piriz J, Mirrione M, Chung C, Proulx CD, Schulz D, Henn F, Malinow R. Synaptic potentiation onto habenula neurons in the learned helplessness model of depression. Nature. 2011a; 470:535–539. [PubMed: 21350486]

Li N, Downey JE, Bar-Shir A, Gilad AA, Walczak P, Kim H, Joel SE, Pekar JJ, Thakor NV, Pelled G. Optogenetic-guided cortical plasticity after nerve injury. Proc Natl Acad Sci U S A. 2011b; 108:8838–8843. [PubMed: 21555573]

Liang Z, King J, Zhang N. Uncovering intrinsic connectional architecture of functional networks in awake rat brain. J Neurosci. 2011; 31:3776–3783. [PubMed: 21389232]

Liang Z, King J, Zhang N. Anticorrelated resting-state functional connectivity in awake rat brain. Neuroimage. 2012a; 59:1190–1199. [PubMed: 21864689]

Liang Z, King J, Zhang N. Intrinsic organization of the anesthetized brain. J Neurosci. 2012b; 32:10183–10191. [PubMed: 22836253]

Liang Z, King J, Zhang N. Neuroplasticity to a single-episode traumatic stress revealed by resting-state fMRI in awake rats. Neuroimage. 2014; 103:485–491. [PubMed: 25193500]

Liang Z, Li T, King J, Zhang N. Mapping thalamocortical networks in rat brain using resting-state functional connectivity. Neuroimage. 2013; 83:237–244. [PubMed: 23777756]

Liang Z, Liu X, Zhang N. Dynamic resting state functional connectivity in awake and anesthetized rodents. Neuroimage. 2015; 104:89–99. [PubMed: 25315787]

Lu H, Zuo Y, Gu H, Waltz JA, Zhan W, Scholl CA, Rea W, Yang Y, Stein EA. Synchronized delta oscillations correlate with the resting-state functional MRI signal. Proc Natl Acad Sci U S A. 2007; 104:18265–18269. [PubMed: 17991778]

Martin C, Martindale J, Berwick J, Mayhew J. Investigating neural-hemodynamic coupling and the hemodynamic response function in the awake rat. Neuroimage. 2006; 32:33–48. [PubMed: 16725349]

Milad MR, Quirk GJ. Fear extinction as a model for translational neuroscience: ten years of progress. Annu Rev Psychol. 2012; 63:129–151. [PubMed: 22129456]

Myers-Schulz B, Koenigs M. Functional anatomy of ventromedial prefrontal cortex: implications for mood and anxiety disorders. Mol Psychiatry. 2012; 17:132–141. [PubMed: 21788943]

Ongur D, Price JL. The organization of networks within the orbital and medial prefrontal cortex of rats, monkeys and humans. Cereb Cortex. 2000; 10:206–219. [PubMed: 10731217]

Perry JL, Joseph JE, Jiang Y, Zimmerman RS, Kelly TH, Darna M, Huettl P, Dwoskin LP, Bardo MT. Prefrontal cortex and drug abuse vulnerability: translation to prevention and treatment interventions. Brain Res Rev. 2011; 65:124–149. [PubMed: 20837060]

Petrides M. Impairments on nonspatial self-ordered and externally ordered working memory tasks after lesions of the mid-dorsal part of the lateral frontal cortex in the monkey. J Neurosci. 1995; 15:359–375. [PubMed: 7823141]

Porrino LJ, Lyons D. Orbital and medial prefrontal cortex and psychostimulant abuse: studies in animal models. Cereb Cortex. 2000; 10:326–333. [PubMed: 10731227]

Ridderinkhof KR, Ullsperger M, Crone EA, Nieuwenhuis S. The role of the medial frontal cortex in cognitive control. Science. 2004; 306:443–447. [PubMed: 15486290]

Ruggiero DA, Mraovitch S, Granata AR, Anwar M, Reis DJ. A role of insular cortex in cardiovascular function. J Comp Neurol. 1987; 257:189–207. [PubMed: 3571525]

Saper CB. Convergence of autonomic and limbic connections in the insular cortex of the rat. J Comp Neurol. 1982; 210:163–173. [PubMed: 7130477]

Saper, CB. The hypothalamus. In: Paxinos, G., editor. The Human Nervous System. Academic Press; San Diego, CA: 2003. p. 513-550.

Scott NA, Murphy TH. Hemodynamic responses evoked by neuronal stimulation via channelrhodopsin-2 can be independent of intracortical glutamatergic synaptic transmission. PLoS One. 2012; 7:e29859. [PubMed: 22253807]

Shin LM, Rauch SL, Pitman RK. Amygdala, medial prefrontal cortex, and hippocampal function in PTSD. Ann N Y Acad Sci. 2006; 1071:67–79. [PubMed: 16891563]

Swanson, LW. Brain Maps: Structure of the Rat Brain. Elsevier; 2004.

Vertes RP. Differential projections of the infralimbic and prelimbic cortex in the rat. Synapse. 2004; 51:32–58. [PubMed: 14579424]

Warden MR, Selimbeyoglu A, Mirzabekov JJ, Lo M, Thompson KR, Kim SY, Adhikari A, Tye KM, Frank LM, Deisseroth K. A prefrontal cortex-brainstem neuronal projection that controls response to behavioural challenge. Nature. 2012; 492:428–432. [PubMed: 23160494]

Yizhar O, Fenno LE, Davidson TJ, Mogri M, Deisseroth K. Optogenetics in neural systems. Neuron. 2011; 71:9–34. [PubMed: 21745635]

Zhang N, Rane P, Huang W, Liang Z, Kennedy D, Frazier JA, King J. Mapping resting-state brain networks in conscious animals. J Neurosci Methods. 2010a; 189:186–196. [PubMed: 20382183]

Zhang N, Zhu XH, Zhang Y, Chen W. An fMRI study of neural interaction in large-scale cortico-thalamic visual network. Neuroimage. 2008; 42:1110–1117. [PubMed: 18598771]

Zhang N, Zhu XH, Zhang Y, Park JK, Chen W. High-resolution fMRI mapping of ocular dominance layers in cat lateral geniculate nucleus. Neuroimage. 2010b; 50:1456–1463. [PubMed: 20114078]

Research Highlights

- Opto-fMRI was used to map the mPFC functional network in awake rats.
- Photo-stimulation of mPFC activated prefrontal, striatal and limbic regions.
- The mPFC network activation pattern revealed by opto-fMRI was robust.
- BOLD signals were substantially reduced when animals were anesthetized.

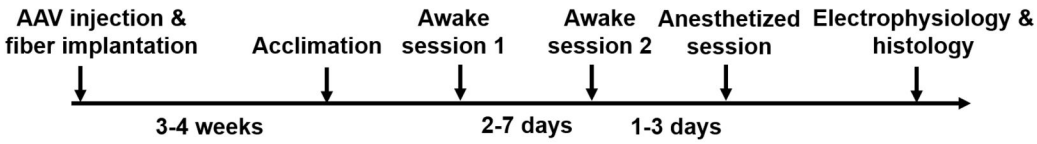

Figure 1.
Schematic diagram illustrating the timeline of the experiment paradigm.

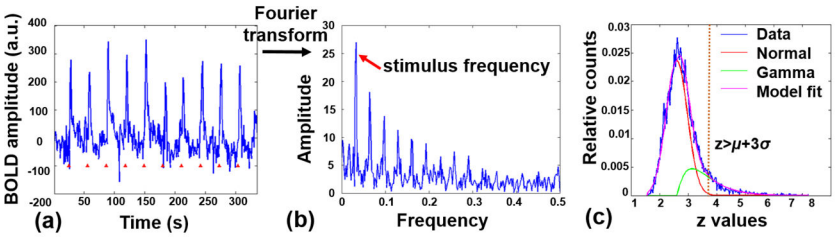

Figure 2.

Procedures for analyzing opto-fMRI data. Left, a representative BOLD time course in response to ten 1-second stimuli delivered at the rate of one stimulus per 30 seconds (red triangles). Middle, the power spectrum of the BOLD time course after Fourier transform. Right, an example of Normal-Gamma model fitting to the distribution of z values of all voxels in a BOLD map. Blue, empirical data, red, fitted Normal distribution, green, fitted Gamma distribution, magenta, fitted model.

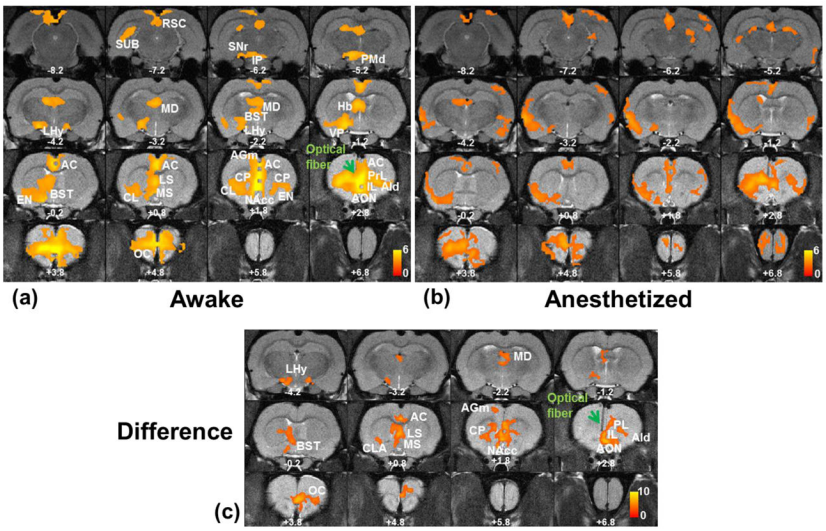

Figure 3.

Averaged activation maps in response to IL optogenetic stimulation. a) The averaged activation map in the awake state. b) The averaged activation map in the anesthetized state. Both maps in a) and b) were displayed at the threshold of $z > \mu + 2\sigma$ (i.e. $p<0.05$ at the whole brain level). c) Statistical comparison of activations maps between the awake and anesthetized states. T values were thresholded at $p<0.001$ (uncorrected). Green arrow, implanted optical fiber. Distance to Bregma is labeled in each slice. AC, anterior cingulate cortex; AGm, medial agranular (frontal) cortex; AId, dorsal agranular insular cortex; AON, anterior olfactory nucleus; BST, Bed nucleus of stria terminalis; CL, claustrum; EN, CP, caudate-putamen; endopiriform nucleus; Hb, habenula; IL, infralimbic; IP, interpeduncular nucleus; LHy, lateral hypothalamus; LS, lateral septum; MD, mediodorsal nucleus; MS, medial septum; NAcc, nucleus accumbens; OC, orbital cortex; PMd, dorsal premammillary nucleus; PrL, prelimbic; SNr, substantia nigra; SUB, subiculum; RSC, retrosplenial cortex.

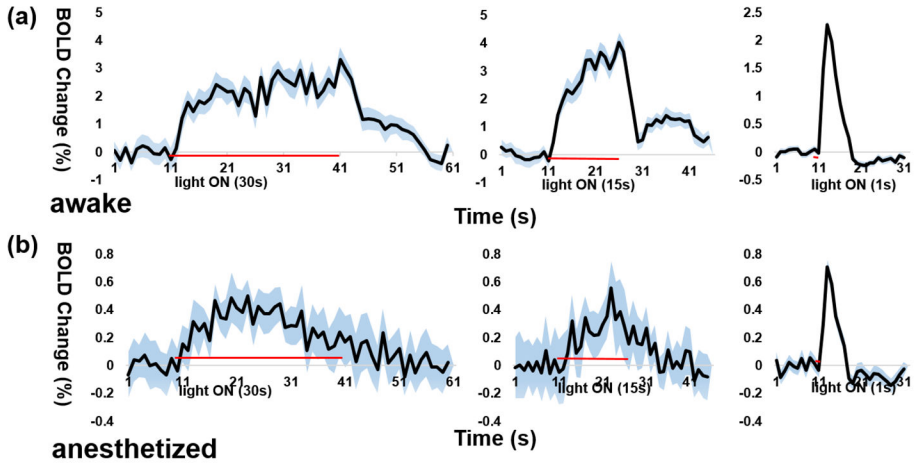

Figure 4.

Time courses of optically-evoked BOLD signals in the anterior cingulate (AC) cortex during awake and anesthetized states. a) Time courses in the awake state. b) Time courses in the anesthetized state. x axis, time (s). y axis, percentage BOLD signal change. Red lines indicate stimulation periods. Blue shades in SEM.

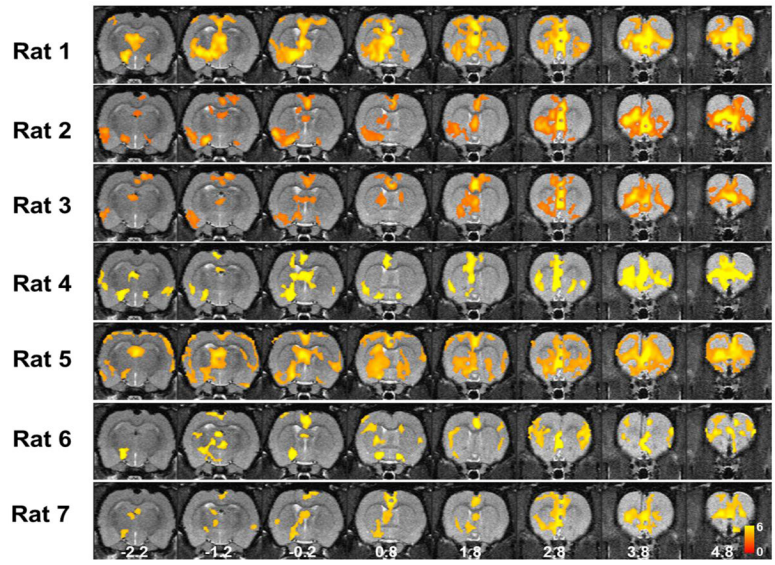

Figure 5a

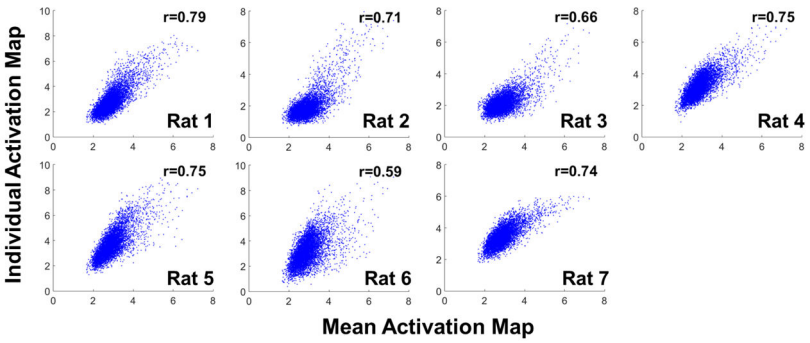

Figure 5b

Figure 5.

a) Activation maps of all individual rats in the awake state. For each rat, two awake sessions were averaged. Maps were thresholded at $z > \mu + 2\sigma$ (i.e. $p<0.05$ at the whole brain level). Distance to Bregma is labeled at the bottom of each slice. b) Voxel-wise correlations of z values between individual BOLD maps and the mean activation map from all animals (i.e. Fig. 3a).

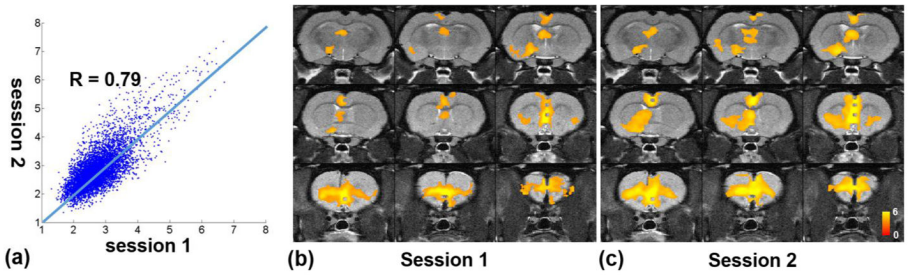

Figure 6.

Consistent activation maps between the first and second awake imaging sessions. a) The voxel-wise correlation of z values between the two awake sessions averaged across all rats. b) The averaged activation map of Session 1. c) The averaged activation map of Session 2.

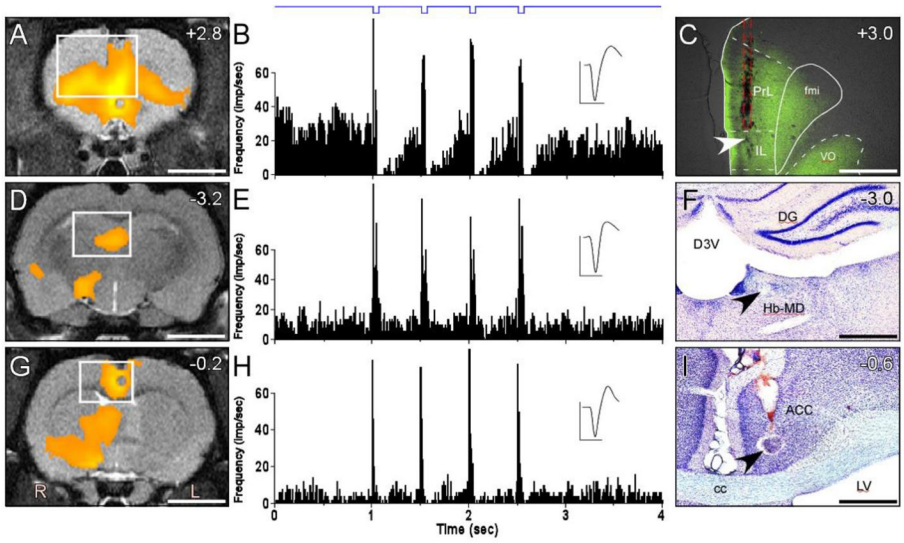

Figure 7.

Photo-stimulation of IL increases neuronal discharges in areas of increased BOLD signaling in the IL network. A, D, and G: Mean BOLD signal change across rats after photo-stimulating IL. White boxes indicate the region in C, F, and I. B and E: PSTH responses of simultaneous recordings from IL (B) and Hb-MD complex (E) during 2-Hz photo-stimulation (blue trace) delivered by an optrode in IL. C: Widefield fluorescent photomicrograph of coronal section showing region of ChR2 expression in IL and placement of optic fiber above IL (red dash outline). White arrow indicates recording site in IL. F: Nissl-stained section shows lesion (black arrow) at recording site in Hb-MD complex. H: PSTH response from photo-stimulating ChR2-expressing IL terminals with optrode in ACC. I: Nissl-stained section shows lesion (black arrow) at recording site in ACC. Scale bars: 4 mm in A, D, and G; 1.25 mm in C; 500 μm in F; 250 μm in I. PSTH bin widths, 10 ms. Mean neuronal waveform scales: 300 μV, 1 ms. ACC, anterior cingulate cortex; D3V, dorsal 3rd ventricle; DG, dentate gyrus; cc, corpus callosum; fmi, forceps minor; Hb-MD, habenula-mediodorsal complex; IL, infralimbic cortex; LV, lateral ventricle; PrL, prelimbic cortex; VO, ventral orbital cortex.